RAD51 Enhances Zygotic Interhomolog Repair

Jonathan J. Wilde[1], Tomomi Aida[1], Martin Wienisch[1], Qiangge Zhang[1], Peimin Qi[1], and Guoping Feng[1,2*]

Affiliations:
[1]McGovern Institute for Brain Research, Department of Brain and Cognitive Sciences, Massachusetts Institute of Technology (MIT), Cambridge, Massachusetts 02139, USA

[2]Stanley Center for Psychiatric Research, Broad Institute of MIT and Harvard, Cambridge, Massachusetts 02142, USA

***Correspondence to G.F.:** fengg@mit.edu

Recent advances in CRISPR/Cas-based genome editing, including three-component CRISPR[1], the use of long single-strand donors[2], enhanced microhomology-mediated end-joining (MMEJ)[3], and pharmacological approaches[4-7] have greatly improved knock-in (KI) efficiency. In our search for factors to further improve KI efficiency for broad therapeutic use and efficient generation of primate disease models, we found that the strand exchange protein RAD51 can significantly increase homozygous KI efficiency using CRISPR/Cas9 in mouse embryos through an interhomolog repair (IHR) mechanism. Using a variety of approaches, we demonstrate robust enhancement of zygotic IHR by RAD51 and show that this can be leveraged both for generating homozygous KI animals from wildtype zygotes with exogenous donors and for converting heterozygous alleles into homozygous alleles without exogenous templates. Thus, our study provides both conclusive evidence supporting the existence of zygotic IHR mechanisms and a new method to significantly improve IHR efficiency for potential therapeutic use.

We previously described a three-component CRISPR approach, which employs Cas9 protein and chemically synthesized crRNA and tracrRNA for efficient KI of transgenes[1,2,8]. Additional published work in rabbit embryos has shown significant enhancement of KI efficiency using RS-1, a chemical agonist of the homology-directed repair (HDR) pathway member RAD51[6]. We began our study by attempting to use a combination of these techniques for high-efficiency knock-in of an autism-associated point mutation in *Chd2* (c.5051G>A; R1685H in human, R1684H in mouse; hereon referred to as *Chd2*^{R1684H}; **Fig. 1a**) using a single-stranded oligonucleotide donor (ssODN). Previous studies have shown that KI efficiency is affected by the proximity of the Cas9 cut site and the insertion site[9], so we chose a guide positioned where the cut site is directly adjacent to the desired G>A point mutation. Genotyping

68 of mouse embryos after pronuclear injection and *in vitro* culture with or without RS-1 (7.5μM)
69 showed a high KI efficiency at the targeted *Chd2* locus, but revealed that RS-1 did not affect KI
70 efficiency (**Extended Data Fig. 1**). Although the known mechanisms of RAD51 function
71 suggest it may not promote knock-in with ssODNs, our previous success using exogenous
72 protein to promote high-efficiency KI[1,2,3,8] and the fact that RS-1 can be highly dosage-sensitive[6]
73 led us to hypothesize that the use of exogenous RAD51 protein in combination with three-
74 component CRISPR could potentially increase KI efficiency. We first performed both pronuclear
75 (PNI) and cytoplasmic (CPI) injections of crRNA, tracrRNA, Cas9, ssODN (30 ng/μL for PNI
76 and 100 ng/μL for CPI), and RAD51 protein in mouse zygotes and genotyped the resulting F_0
77 pups (example chromatograms in **Fig. 1b**). In 18 pups, we observed an overall KI efficiency of
78 61.1% (**Fig. 1c**) and, surprisingly, a homozygous KI efficiency of 55.5% (**Fig. 1d**). We did not
79 observe significant differences in efficiency between CPI and PNI (**Extended Data Fig. 2**), so
80 we focused on PNI for the remainder of this study. Although we performed all genotyping of
81 these animals using primers sitting outside of the homology arms, we could not rule out the
82 possibility that the homozygous animals were actually compound heterozygotes with large
83 deletions encompassing the cut site on one allele[10]. We therefore bred 6 of the F_0 homozygous
84 KI mice with wildtype C57BL/6N animals and genotyped the resulting F_1 progeny. Sanger
85 sequencing showed that all 36 F_1 pups were heterozygous mutants, confirming the homozygosity
86 of F_0 animals (**Fig. 1e**).
87 Since we did not initially generate *Chd2*^{R1684H} mice with injections lacking RAD51, we
88 performed additional injections to directly assess the ability of RAD51 to increase KI efficiency.
89 Zygotic injections were performed with and without RAD51, embryos were cultured for two
90 days, and nested PCR was performed for genotyping. Sanger sequencing revealed that RAD51

91 only slightly increased overall KI efficiency (**Fig. 2a**, left, $p<0.05$, one-tailed chi-square test), but
92 drastically increased homozygous KI efficiency (**Fig. 2a, right**, $p<0.0001$, one-tailed chi-square
93 test). It is widely accepted that CRISPR/Cas9-mediated editing efficiency can be highly locus-
94 and guide-dependent, so we investigated the effects of RAD51 at a second genomic locus to
95 confirm its efficacy. Using the same injection strategy employed for *Chd2*, we attempted to
96 knock in an albinism-associated human mutation (c.265T>A; C89S; hereon referred to as
97 Tyr^{C89S}; schematic in **Fig. 2b**) in the *Tyr* gene[11], which encodes for tyrosinase, the rate-limiting
98 enzyme in melanin production. Albinism is a recessive disorder and, as such, only homozygous
99 mutation of *Tyr* results in mice completely lacking pigment (**Fig. 2c, d**). However, indel-induced
100 disruption of *Tyr* can also result in albinism, so all F_0 animals were genotyped to assess the
101 effects of RAD51. Injections without RAD51 showed a high overall KI efficiency, but this
102 efficiency was not significantly affected by the addition of RAD51 (**Fig. 2e, left**). However, our
103 genotyping results again indicated that RAD51 can significantly increase homozygous KI
104 efficiency, with 44.4% of pups exhibiting an albino phenotype resulting from homozygous KI of
105 the Tyr^{C89S} allele with RAD51, as compared to only 12% without (**Fig. 2e, right**).
106 Strikingly, RAD51 co-injection more than doubled the observed homozygosity at both
107 the *Chd2* and *Tyr* loci (**Fig. 2a, e**). Previous attempts to increase HDR through pharmacological
108 or genetic mechanisms have not shown such high homozygosity rates[7,9,12], leading us to question
109 the mechanism by which RAD51 can promote such an outcome. Our evidence that RAD51 does
110 not strongly affect overall efficiency of ssODN-mediated knock-in (**Fig. 2a,d**) suggested that its
111 effects on homozygosity do not come from directly increasing independent KI events on both
112 alleles. Additionally, due to the random nature of insertion-deletions (indels) produced by non-
113 homologous end joining (NHEJ), we found it surprising that we observed multiple embryos from

114 both *Chd2*^{R1684H} and *Tyr*^{C89S} injections whose genotyping results suggested the presence of the
115 same indel on both alleles (**Extended Data Fig. 3**). Genotyping of F_1 pups derived from a female
116 with such a homozygous indel revealed that all pups were heterozygous for the same indel,
117 indicating that the phenomenon was not due to an indel on one allele and a large deletion
118 encompassing the cut site on the other (**Extended Data Fig. 3**). Although we could not rule out
119 that these deletions were generated by MMEJ, which can result in stereotyped indels based on
120 local homology[3,13], the variety of observed indels suggested that the homozygosity resulted from
121 recombination between homologs that transferred the KI or indel allele from one chromosome to
122 the other.

123 More than 20 years ago, experiments in mouse ES cells found evidence of recombination
124 events between homologous chromosomes[14,15]. While these interhomolog repair (IHR) events
125 are now well-understood in meiotic cells, their occurrence in zygotes and somatic cells is poorly
126 described. However, recently published data from experiments attempting to correct a 4bp
127 GAGT deletion in *MYBPC3* in human embryos support a potential zygotic IHR mechanism
128 whereby one allele can serve as the repair template for the other after induction of a targeted
129 double-strand break (DSB) by Cas9[16]. Based on these data, we hypothesized that RAD51
130 promotes homozygous KI through a similar mechanism. To test this, we first performed PNI
131 using an injection mixture containing an equimolar ratio of two separate ssODNs containing
132 different point mutations at the same loci, allowing us to identify independent knock-in events
133 via the observation of compound heterozygosity (**Fig. 3a**). In line with our previous observations
134 (**Fig. 2a**), we found that co-injection of RAD51 significantly increased homozygous KI
135 efficiency **(Fig. 3b)**. Strikingly, compound heterozygosity was observed in 5/12 control embryos
136 with a KI event on both alleles, but was not observed in any RAD51-injected embryos (**Fig. 3b**),

137 supporting our hypothesis that RAD51 increases homozygosity through an enhanced IHR
138 mechanism. Importantly, we did not observe significant differences in overall KI rates between
139 the two ssODNs (**Extended Data Fig. 4**), ruling out the possibility that our observations were
140 due to a bias toward one donor over the other.

141 In order to more directly test the IHR mechanism, we attempted to generate homozygous
142 *Chd2*^{R1684H} embryos without the use of an exogenous donor through homozygous conversion.
143 Using *in vitro* fertilization (IVF) with wildtype C57Bl/6N eggs and sperm from homozygous
144 *Chd2*^{R1684H} male mice, we generated heterozygous zygotes and specifically targeted Cas9 to the
145 maternal *Chd2* locus. As illustrated in **Figure 3c**, PNI was performed on zygotes at ~8 hours post
146 fertilization (hpf) using a mixture of crRNA, tracrRNA, and Cas9 with or without RAD51.
147 Because the *Chd2*^{R1684H} allele contains mutations in both the guide sequence and its associated
148 PAM, Cas9 is only capable of cutting the wildtype maternal allele (**Extended Data Fig. 5**).
149 Therefore, by omitting the donor template from the injection mixture we were able to directly
150 test both the rate of baseline CRISPR/Cas9-mediated IHR in the zygote and the ability of
151 RAD51 to enhance such a mechanism. In support of data published by Ma *et al*., we observed
152 IHR events in 26% of control-injected embryos (**Fig. 3d,e**). Strikingly, co-injection of RAD51
153 was capable of increasing this rate to 74% (**Fig. 3e**). To directly rule out the possibility of false
154 positives resulting from monoallelic deletions on the maternal allele, we developed and
155 performed a genomic qPCR assay to analyze copy number at the targeted locus (**see Methods**).
156 First, using genomic DNA from wildtype mice and *Shank3B*$^{+/-}$ mice harboring a heterozygous
157 deletion of exon 13 of *Shank3*[17], we confirmed that our method was capable of identifying
158 heterozygous deletions **(Fig. 3f)**. Using the same assay design, we confirmed that 5 of 5

159 randomly selected homozygous mutants carried 2 copies of the *Chd2* locus (**Fig. 3f**), validating
160 our conclusion that RAD51 enhances zygotic IHR.

161 Our data demonstrate that RAD51 enhances interhomolog repair and that this
162 enhancement can be leveraged for both donor-free homozygous conversion and *de novo*
163 homozygous KI. To our knowledge, our results are also the first to definitively show the
164 existence of IHR events in mammalian zygotes. Although previous work has suggested the
165 existence of these events, a recent commentary in *bioRxiv* highlights the need for more rigorous
166 analyses to confirm such findings and outlines 3 main points[18]. First, Egli *et al.* argue that
167 because IHR requires physical interaction of the maternal and paternal genomes, there must be a
168 sufficient explanation for how IHR can result from Cas9-mediated DSBs that occur while the
169 maternal and paternal genomes are segregated in separate pronuclei. Second, they suggest that
170 parthenogenesis must be ruled out as a possibility for the observed loss-of-heterozygosity. Last,
171 they suggest that additional measures be taken to rule out the possibility that the observed loss-
172 of-heterozygosity is due to large NHEJ-induced indels emanating from the Cas9 cut site. Our
173 data fulfills all three requirements and further goes on to show that RAD51 is capable of
174 significantly enhancing IHR. With respect to the need for physical proximity between homologs
175 to allow IHR, previous kinetic studies have shown that Cas9 can remain bound to its cut site for
176 up to 6 hours[19], which would be long enough to allow mitotic association of the maternal and
177 paternal alleles in mouse zygotes. Furthermore, an additional study in mouse demonstrated
178 successful correction of a disease mutation in zygotes without the use of exogenous donor
179 DNA[20], supporting the existence of a zygotic IHR mechanism. With regard to the ruling out
180 parthenogenesis, our experimental design relied upon transfer of the paternal mutation to the
181 maternal allele, excluding the possibility of a parthenogenesis-based mechanism. Last,

182 previously published work mouse zygotes showed that the median deletion size associated with a
183 Cas9-induced cut with a single sgRNA was ~10bp, that deletions do not surpass 600bp, and that
184 the occurrence of large deletions (>100bp) was largely sequence-dependent and far too
185 infrequent to account for the high rates of IHR observed in our experiments[10]. In accordance with
186 these findings, our copy-number analyses and F_1 genotyping data rule out large deletions as the
187 source of loss-of-heterozygosity and therefore support our conclusions regarding the existence
188 and enhancement of zygotic IHR.

189 Together, our studies validate the existence of a bona fide IHR-based DSB repair
190 mechanism in the mammalian zygote and demonstrate significant enhancement of this process
191 by the HDR-associated strand exchange factor RAD51. Furthermore, we show that enhancement
192 of the IHR and/or HDR pathways with exogenous RAD51 can be used for highly efficient
193 homozygous KI and donor-free homozygous conversion. Ongoing efforts to generate primate
194 models of human diseases have been hindered by low efficiency, long generation times, and high
195 costs associated with obtaining homozygotes. However, our method has the potential to generate
196 F_0 homozygotes with high efficiency, significantly decreasing costs and study length. Taken as a
197 whole, our findings have broad implications for applications in basic sciences, disease modeling,
198 therapeutic gene editing, and biotechnology.

199

200

201 **Methods**

202 ***Data Availability:*** The raw data supporting the findings in this manuscript can be obtained from
203 the corresponding author upon reasonable request.

204 ***Animal Care and Use***: All mouse work was performed with the supervision of the
205 Massachusetts Institute for Technology Division of Comparative Medicine (DCM) under
206 protocol 0416-024-19, which was approved by the Committee for Animal Care (CAC). All
207 procedures were in accordance with the guidelines set forth by the Guide for Care and Use of
208 Laboratory Animals, National Research Council, 1996 (institutional animal assurance no. A-
209 3125-01). All embryos injected for the experiments described in this manuscript were on a
210 C57BL/6NTac background (Taconic; referred to as C57BL/6N in paper).
211 ***Preparation of Injection Mixtures***: tracrRNA, crRNAs, and ssODNs were synthesized by
212 Integrated DNA Technologies (see Supplementary Table 1 for sequences). All injection mixtures
213 were prepared in a final volume of 50µL according using the same protocol. Using RNase-free
214 water, reagents, and consumables, crRNA (final concentration 0.61µM), tracrRNA (final
215 concentration 0.61µM), and ultrapure Tris-HCl, pH7.39 (final concentration 10mM,
216 ThermoFisher) were mixed and incubated at 95°C for 5 minutes. The mixtures were cooled to
217 room temperature for 10 minutes on the benchtop and then EnGen Cas9-NLS (New England
218 Biolabs) was added to a final concentration of 30ng/µL. The mixtures were incubated at 37°C for
219 15 minutes before adding any remaining components: ssODN (final concentration 30ng/µL),
220 RAD51 (Creative Biomart, final concentration 10ng/µL). Injection mixtures were stored on ice
221 and briefly heated to 37°C prior to injection. For experiments utilizing RS-1, embryos were
222 cultured in KSOM-AA with 7.5µM RS-1 (Sigma) or DMSO (Sigma, 1:1000) for 24 hours,
223 washed, and cultured in standard FHM until collection for genotyping.
224 ***In Vitro Fertilization***: *In vitro* fertilization was performed using FERTIUP® Mouse
225 Preincubation Medium and CARD MEDIA (Kyudo Company) according to the manufacturer's
226 protocol.

227 ***Zygotic Injections:*** Female mice (4-5 weeks old, C57BL/6NJ) were superovulated by IP
228 injection of PMS (5 IU/mouse, three days prior to microinjection) and hCG (5 IU/mouse, 47
229 hours after PMS injection), and paired with males. Plugged females were sacrificed by cervical
230 dislocation at day 0.5pcd and zygotes were collected into 0.1% hyaluronidase/FHM. Zygotes
231 were washed in drops of FHM and cumulus cells were removed. Zygotes were cultured in
232 KSOM-aa medium for one hour and used for microinjection. Pronuclear injection was performed
233 using a micromanipulator (Narishige), microscope (Nikon), and injector (Eppendorf). Zygotes
234 were cultured until collection for genotyping. For experiments giving rise to F_0 animals, embryos
235 were surgically implanted into pseudopregnant CD-1 females (Charles River Laboratories, Strain
236 Code 022) 24 hours post-injection, allowed to develop normally, and recovered following natural
237 birth.
238 ***Embryo DNA Purification***: Embryos were collected at morula stage in 6µL embryo digestion
239 buffer (125µg/mL proteinase K, 100mM Tris-HCl pH 8.0, 100mM KCl, 0.02% gelatin, 0.45%
240 Tween-20, 60µg/mL yeast tRNA) and digested for 1 hour at 56°C. Proteinase K was inactivated
241 via incubation at 95°C for 10 minutes. Embryo DNA was stored at -20°C until use.
242 ***Tail DNA Purification***: Tail snips (~0.5cm length) were collected from animals, placed in 75µL
243 alkaline lysis buffer (25mM NaOH, 0.2mM EDTA), and incubated at 95°C for 30 minutes.
244 Digestion was stopped via addition of 75µL neutralization buffer (40mM Tris-HCl pH 5.0).
245 Samples were stored at 4°C until genotyping.
246 ***Chd2^{R1684H} Genotyping*:** Initial PCR was performed using either 3µL embryo DNA or 2µL
247 purified tail DNA. The longer amplification of the nested PCR reaction was performed using the
248 Chd2-RH_Long_F/R primer pair listed in Supplementary Table 2 and an annealing temperature

249 of 65°C. Nested PCR was performed using 2µL of the initial 25µL PCR reaction, the Chd2-
250 RH_F/R primer pair listed in Supplementary Table 2, and an annealing temperature of 65°C.
251 ***Tyr^{C89S} Genotyping:*** Initial PCR was performed using 2µL purified tail DNA. The longer
252 amplification of the nested PCR reaction was performed using the Tyr_Long_F/R primer pair
253 listed in Supplementary Table 2 and an annealing temperature of 65°C. Nested PCR was
254 performed using 2µL of the initial 25µL PCR reaction, the Tyr_F/R primer pair listed in
255 Supplementary Table 2, and an annealing temperature of 65°C.
256 ***Genomic qPCR****:* To determine copy number at specific genomic loci, we developed a strategy
257 utilizing multiplex nested qPCR. We first performed multiplex amplification of both the edited
258 *Chd2* region and a region of the *Gapdh* promoter, which is located on a different chromosome, in
259 a short round of PCR (10 cycles). In the case of our *Shank3B* control experiment, we attempted
260 to match the input DNA concentration used for experiments utilizing DNA from cultured
261 embryos. Based on an estimation of ~6pg DNA per cell and a PCR input of ~30 cells, we used
262 180pg *Shank3B*$^{+/+}$ or *Shank3B*$^{+/-}$ genomic DNA per initial reaction. We then used the PCR
263 products from the initial multiplex PCR as input for subsequent qPCR using Sso Advanced
264 SYBR Green Supermix (Bio-Rad). qPCR was performed on a CFX96 Touch Real-Time PCR
265 Detection System (Bio-Rad) and analyzed using CFX Maestro software (Bio-Rad). *Chd2* or
266 *Shank3B* signal was normalized to *Gapdh* signal to control for input and a second diploid locus.
267 ***Statistical Analyses***: Statistical analyses were performed using Prism 6 (Graphpad). For initial
268 experiments in which the effects of RS-1 and RAD51 were unknown, as well as mixed oligo KI
269 experiments where RAD51 could potentially increase either compound heterozygosity or
270 homozygosity, two-tailed analyses were used. All other experiments exploring RAD51's ability

271 to increase KI and homozygous KI efficiencies utilized one-tailed tests. Genomic qPCR

272 performed in Figure 3 was analyzed by unpaired t-test. The graph displays mean±SEM.

273

274 **References**

275

276 1. Aida, T. *et al.* Cloning-free CRISPR/Cas system facilitates functional cassette knock-in in
277 mice. *Genome Biol* **16,** 87 (2015).
278 2. Quadros, R. M. *et al.* Easi-CRISPR: a robust method for one-step generation of mice
279 carrying conditional and insertion alleles using long ssDNA donors and CRISPR
280 ribonucleoproteins. *Genome Biol* **18,** 103 (2017).
281 3. Aida, T. *et al.* Gene cassette knock-in in mammalian cells and zygotes by enhanced
282 MMEJ. *BMC Genomics* **17,** 183 (2016).
283 4. Yu, C. *et al.* Small Molecules Enhance CRISPR Genome Editing in Pluripotent Stem
284 Cells. *Cell Stem Cell* **16,** 142–147 (2015).
285 5. Li, G. *et al.* Small molecules enhance CRISPR/Cas9-mediated homology-directed genome
286 editing in primary cells. *Sci. Rep.* **7,** 8943 (2017).
287 6. Song, J. *et al.* RS-1 enhances CRISPR/Cas9- and TALEN-mediated knock-in efficiency.
288 *Nature Communications* **7,** 10548 (2016).
289 7. Maruyama, T. *et al.* Increasing the efficiency of precise genome editing with CRISPR-
290 Cas9 by inhibition of nonhomologous end joining. *Nature Biotechnology* **33,** 538–542
291 (2015).
292 8. Ma, X. *et al.* CRISPR/Cas9-mediated gene manipulation to create single-amino-acid-
293 substituted and floxed mice with a cloning-free method. *Sci. Rep.* **7,** 42244 (2017).
294 9. Paquet, D. *et al.* Efficient introduction of specific homozygous and heterozygous
295 mutations using CRISPR/Cas9. *Nature* **533,** 125–129 (2016).
296 10. Shin, H. Y. *et al.* CRISPR/Cas9 targeting events cause complex deletions and insertions at
297 17 sites in the mouse genome. *Nature Communications* **8,** 15464 (2017).
298 11. Ghodsinejad Kalahroudi, V. *et al.* Two Novel Tyrosinase (TYR) Gene Mutations with
299 Pathogenic Impact on Oculocutaneous Albinism Type 1 (OCA1). *PLoS ONE* **9,** e106656
300 (2014).
301 12. Takayama, K. *et al.* Highly efficient biallelic genome editing of human ES/iPS cells using
302 a CRISPR/Cas9 or TALEN system. *Nucleic Acids Research* **45,** 5198–5207 (2017).
303 13. McVey, M. & Lee, S. E. MMEJ repair of double-strand breaks (director's cut): deleted
304 sequences and alternative endings. *Trends in Genetics* **24,** 529–538 (2008).
305 14. Richardson, C., Moynahan, M. E. & Jasin, M. Double-strand break repair by
306 interchromosomal recombination: suppression of chromosomal translocations. *Genes &*
307 *Development* **12,** 3831–3842 (1998).
308 15. Moynahan, M. E. & Jasin, M. Loss of heterozygosity induced by a chromosomal double-
309 strand break. *Proc Natl Acad Sci USA* **94,** 8988–8993 (1997).
310 16. Ma, H. *et al.* Correction of a pathogenic gene mutation in human embryos. *Nature* **548,**
311 413–419 (2017).
312 17. Peca, J. *et al.* Shank3 mutant mice display autistic-like behaviours and striatal
313 dysfunction. *Nature* **472,** 437–442 (2011).

18. Egli, D., Zuccaro, M., Kosicki, M., Church, G. & Bradley, A. Inter-homologue repair in fertilized human eggs? *bioRxiv* (2017). doi:10.1101/181255
19. Richardson, C. D., Ray, G. J., DeWitt, M. A., Curie, G. L. & Corn, J. E. Enhancing homology-directed genome editing by catalytically active and inactive CRISPR-Cas9 using asymmetric donor DNA. *Nature Biotechnology* **34,** 339–344 (2016).
20. Wu, Y. *et al.* Correction of a Genetic Disease in Mouse via Use of CRISPR-Cas9. *Cell Stem Cell* **13,** 659–662 (2013).

Acknowledgements

The experiments described in this manuscript were funded by the Tan-Yang Center for Autism Research at MIT and the Poitras Center for Affective Disorders Research at MIT. We would like to thank Tetsushi Sakuma and Takashi Yamamoto of Hiroshima University for sharing their knock-in enhancer screening data. Lastly, we are grateful for the helpful discussion and insight provided by members of the Feng lab.

Author Contributions

J.J.W., T.A., M.W., Q.Z., and G.F. designed experiments. J.J.W. and P.Q. performed experiments. J.J.W., T.A., M.W., and G.F. analyzed data. J.J.W., T.A., and G.F. prepared the manuscript.

Competing Financial Interests

The authors of this manuscript declare no competing financial interests.

Materials and Correspondence

Correspondence and materials requests should be addressed to G.F. at fengg@mit.edu

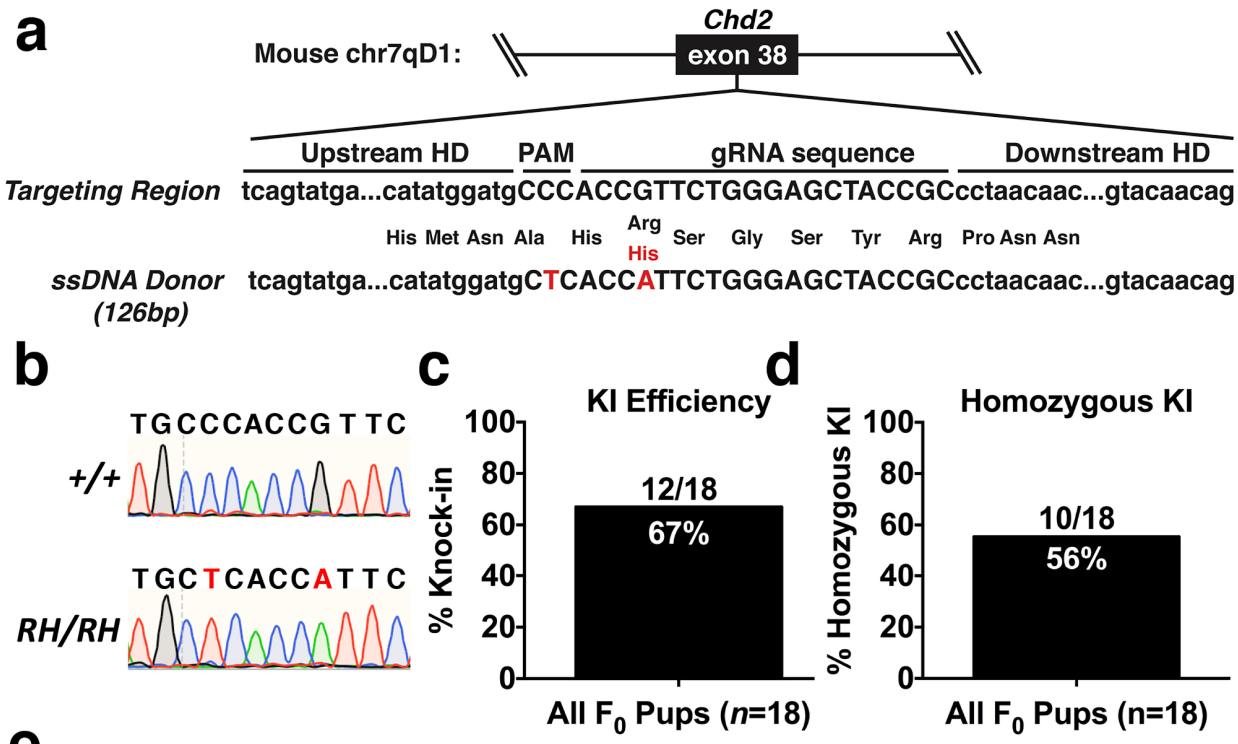

e

Father ID (Genotype)	Mother ID (Genotype)	F_1 Het Pups
C57BL/6N (+/+)	9989 (*RH/RH*)	8/8
C57BL/6N (+/+)	9991 (*RH/RH*)	4/4
C57BL/6N (+/+)	9995 (*RH/RH*)	6/6
9992 (*RH/RH*)	C57BL/6N (+/+)	6/6
9994 (*RH/RH*)	C57BL/6N (+/+)	9/9
10000 (*RH/RH*)	C57BL/6N (+/+)	3/3

Figure 1: Efficient homozygous knock-in with RAD51. a, Schematic of the targeting locus and HR donor for generating *Chd2*^{R1684H} mutant mice. HR donor contains both the c.5051G>A point mutation and a synonymous mutation that destroys the relevant PAM site (HD=homology domain). **b,** Example chromatograms of wildtype (top) and *Chd2*$^{R1684H/R1684H}$ animals (RH=R1684H). **c,** Overall KI efficiency observed in F_0 pups (pups with ≥1 KI allele/total pups). **d,** Homozygous KI rate observed in F_0 pups. **e,** Genotyping results from F_1 pups derived from crosses between F_0 *Chd2*$^{R1684H/R1684H}$ animals and wildtype C57BL/6N animals.

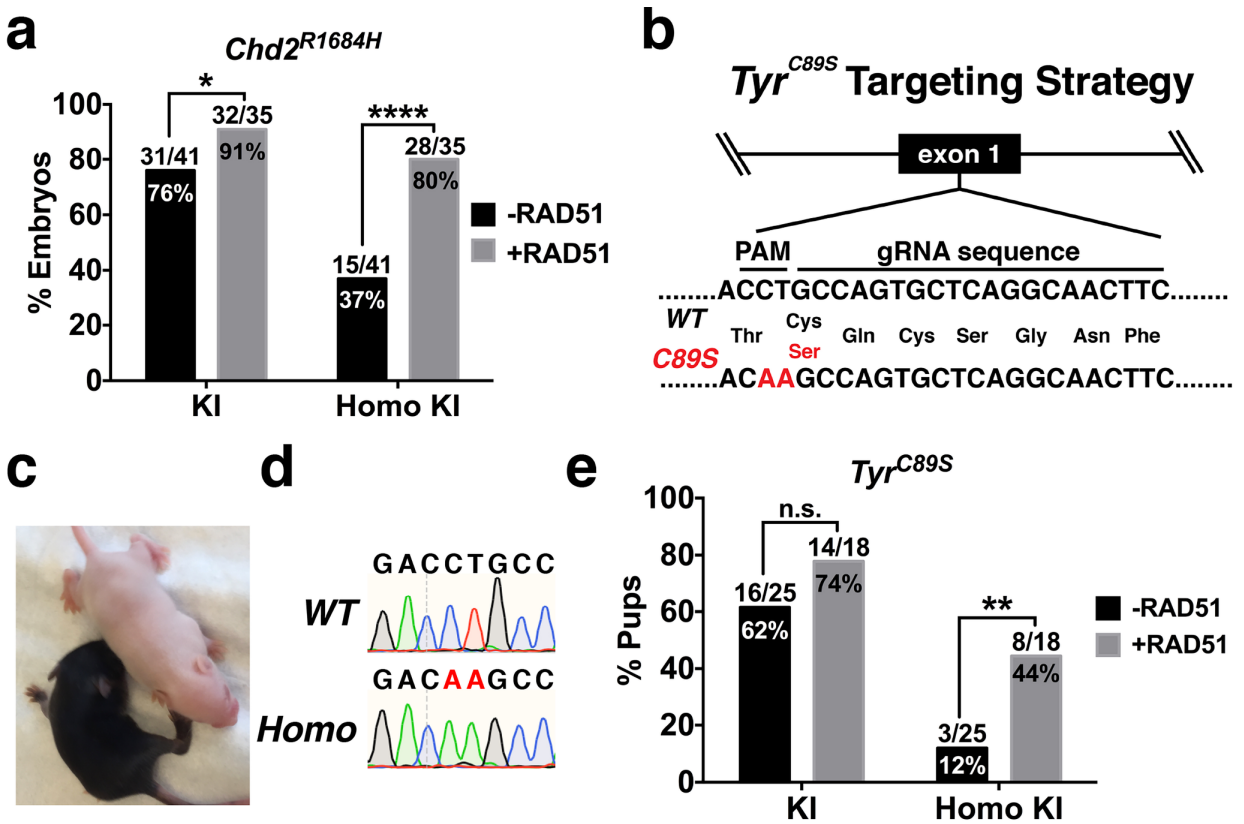

Figure 2: Exogenous RAD51 enhances KI efficiency at multiple loci. a, *Chd2*^{R1684H} PNI using 30ng/µL ssODN with or without RAD51 revealed a slight increase in overall KI efficiency ($p<0.05$, one-tailed chi-square test) and a dramatic increase in homozygous KI efficiency ($p<0.0001$, one-tailed chi-square test). **b,** Schematic of knock-in strategy for the albinism-associated *Tyr*^{C89S} mutation. **c,** Representative examples of *Tyr*$^{+/+}$ (black) and *Tyr*$^{C89S/C89S}$ (white) littermates derived from three-component CRISPR injections using exogenous RAD51. **d,** Representative chromatograms from *Tyr*$^{+/+}$ (top) and *Tyr*$^{C89S/C89S}$ animals. **e,** Genotyping of F_0 animals generated by three-component CRISPR with or without RAD51 showed no significant effect of RAD51 on overall KI efficiency (n.s.=not significant, $p=0.166$, one-tailed chi-square test), but a significant RAD51-dependent increase in homozygous KI rates ($p=0.0081$, one-tailed chi-square test).

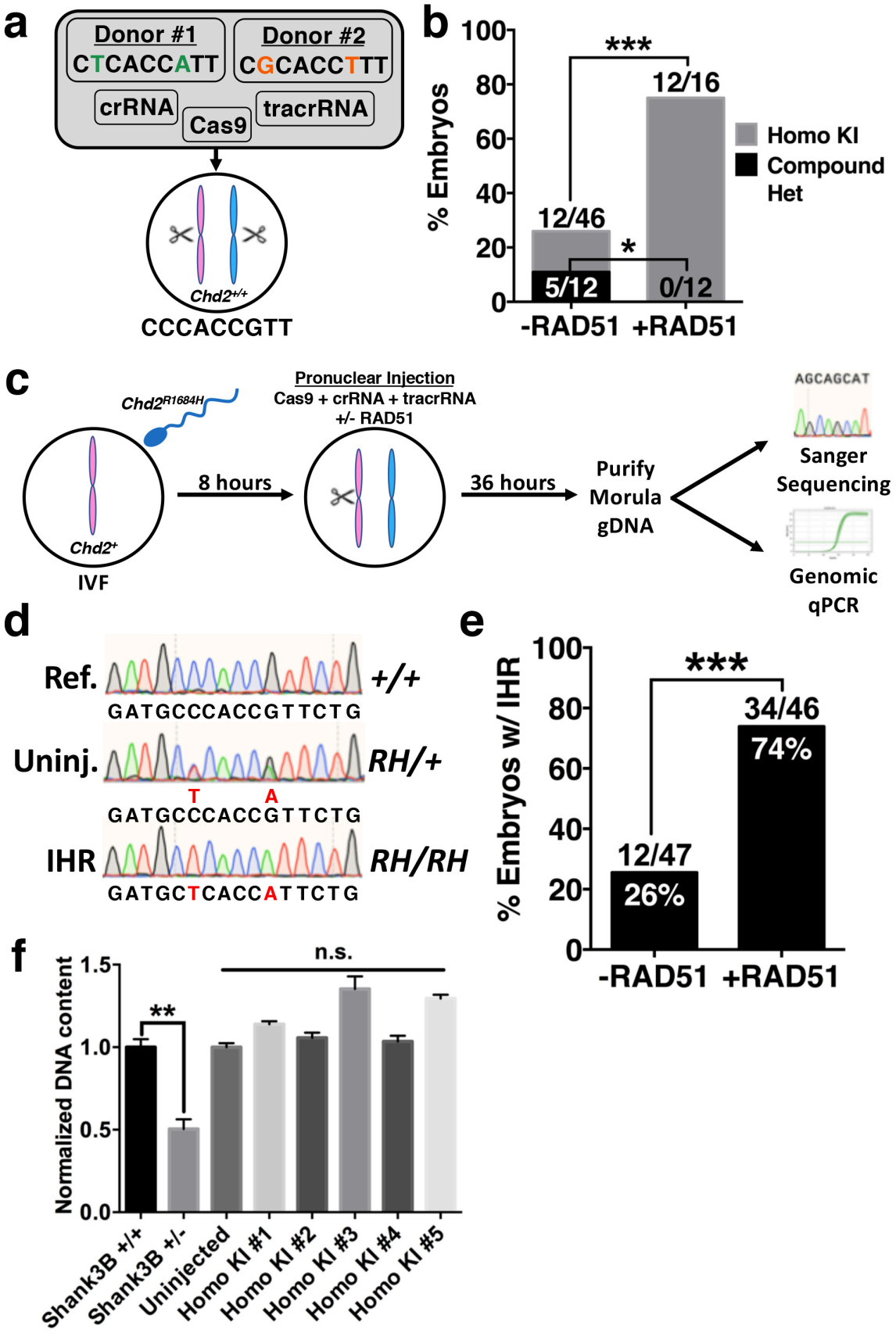
a
Donor #1
CTCACCATT
Donor #2
CGCACCTTT
crRNA
Cas9
tracrRNA
Chd2+/+
CCCACCGTT
b
% Embryos
100
80
60
40
20
0
***
12/16
12/46
*
5/12
0/12
Homo KI
Compound Het
-RAD51
+RAD51
c
Chd2R1684H
Chd2+
IVF
8 hours
Pronuclear Injection
Cas9 + crRNA + tracrRNA
+/- RAD51
36 hours
Purify Morula gDNA
AGCAGCAT
Sanger Sequencing
Genomic qPCR
d
Ref.
+/+
GATGCCCACCGTTCTG
Uninj.
RH/+
T
A
GATGCCCACCGTTCTG
IHR
RH/RH
GATGCTCACCATTCTG
e
% Embryos w/ IHR
100
80
60
40
20
0
***
34/46
74%
12/47
26%
-RAD51
+RAD51
f
Normalized DNA content
1.5
1.0
0.5
0.0
**
n.s.
Shank3B +/+
Shank3B +/-
Uninjected
Homo KI #1
Homo KI #2
Homo KI #3
Homo KI #4
Homo KI #5

365

366 **Figure 3: RAD51 enhances interhomolog repair. a,** Schematic of strategy to test homozygous
367 KI mechanism. Fertilized embryos were injected with Cas9 protein, crRNA, tracrRNA, and an
368 equimolar mixture of two ssODNs varying by two nucleotides with or without RAD51 protein.
369 **b,** Genotyping results from embryos collected following mixed ssODN injection. Homozygous
370 KI efficiency represents the fraction of homozygous KI events observed in all injected embryos
371 (p=0.0008, one-tailed chi-square test). Compound heterozygous rates represent the fraction of
372 homozygous KI embryos with a different KI event on each allele (p=0.0120, two-tailed chi-
373 square test). **c,** Schematic of strategy for testing RAD51-enhanced IHR. Wildtype C57BL/6N
374 eggs were fertilized *in vitro* by sperm collected from male *Chd2*$^{R1684H/R1684H}$ mice and cultured
375 for 8 hours. At 8hpf, PNI was performed with Cas9 protein, crRNA, and tracrRNA with or
376 without RAD51 protein. Since *R1684H* mutants carry a mutation in the PAM associated with the
377 crRNA utilized in these experiments, Cas9 is only capable of cutting the maternal allele. Injected
378 embryos were then cultured for 48 hours and collected at morula stage. Half of the purified DNA
379 was used for nested PCR and Sanger sequencing and the other half was used for multiplex PCR
380 and subsequent qPCR to analyze genomic copy number at the *Chd2* editing locus. **d,**
381 Representative chromatograms showing the wildtype reference sequence (Ref., top), an
382 uninjected *Chd2*$^{R1684H/+}$ embryo generated by IVF (Uninj., middle), and a *Chd2*$^{R1684H/R1684H}$
383 homozygous mutant (IHR, bottom) generated via donor-free, RAD51-enhanced three-component
384 CRISPR. **e,** Sanger sequencing of IVF-derived embryos revealed a significant increase in IHR in
385 embryos injected with RAD51 (p<0.0001, one-tailed chi-square test). **f,** Genomic qPCR targeting
386 *Shank3B* using 180pg genomic DNA from wildtype and *Shank3B*$^{+/-}$ mice indicate that our copy-
387 number strategy is capable of identifying heterozygous deletions (lanes 1-2, p=0.00295, unpaired
388 t-test, t=6.47, df=4, *n*=3 technical replicates per sample, error bars=SEM). qPCR using DNA
389 from an uninjected embryo and 5 randomly selected homozygous *Chd2*^{R1684H} embryos revealed
390 normal copy number at the *Chd2* editing locus in all animals (lanes 3-8, p>0.05, unpaired t-test,
391 t=4.60, df=6, *n=4* technical replicates per sample, error bars=SEM)**.**
392
393
394
395
396

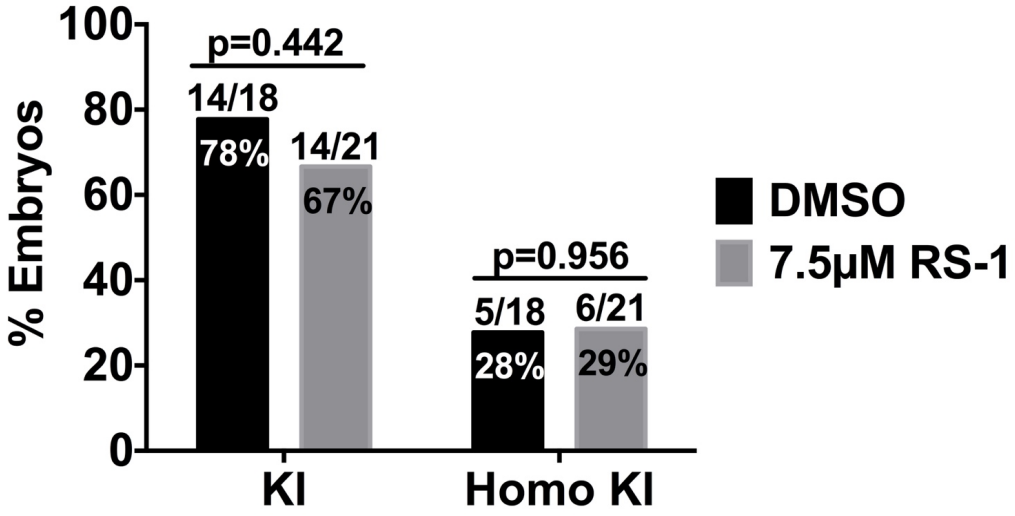

Extended Data Figure 1: RS-1 does not alter KI efficiency in mouse zygotes. Genotyping of morula-stage embryos cultured for 24 hours in either DMSO (1:1000 final concentration) or 7.5μM RS-1 showed no significant difference in overall KI efficiency or homozygous KI efficiency (two-tailed chi-square test).

a

Sex	Injection Type	Genotype	Notes
Female	CPI	RH/RH	
Female	CPI	RH/Indel	
Female	CPI	RH/RH	
Male	CPI	RH/RH	
Male	CPI	RH/RH	
Female	CPI	Indel/Indel	Same Indel
Female	CPI	RH/Indel	
Female	CPI	RH/RH	
Male	CPI	Indel/Indel	Different Indels
Female	PNI	RH/RH	
Male	PNI	RH/RH	
Male	PNI	RH/RH	
Female	PNI	Indel/Indel	Different Indels
Male	PNI	Indel/Indel	Same Indel
Male	PNI	RH/RH	
Male	PNI	Indel/Indel	Same Indel
Female	PNI	Indel/Indel	Same Indel
Female	PNI	RH/RH	

b

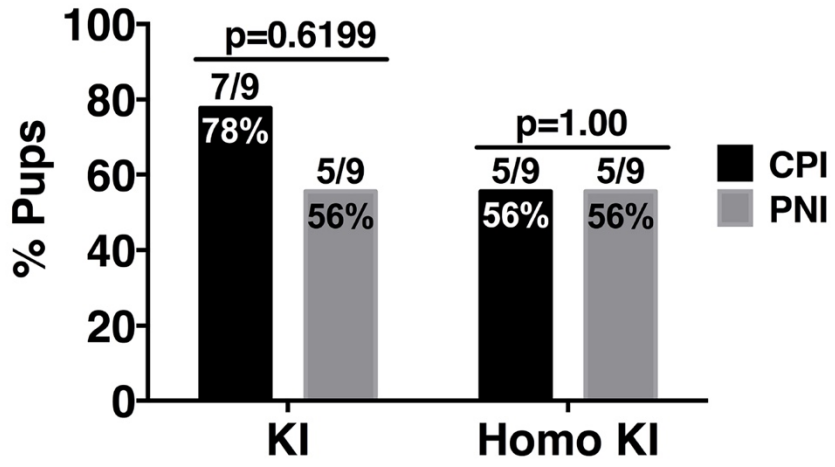

Extended Data Figure 2: Confirmation of F_0 homozygosity. a, Genotyping results for all F_0 pups obtained from either cytoplasmic (CPI) or pronuclear (PNI) injections for *Chd2*^{R1684H} knock-in experiments described in Figure 1. **b,** Quantification of overall KI efficiency (left) and homozygous KI efficiency (right) shows no significant difference in KI rates when comparing CPI and PNI strategies (two-tailed chi-square test).

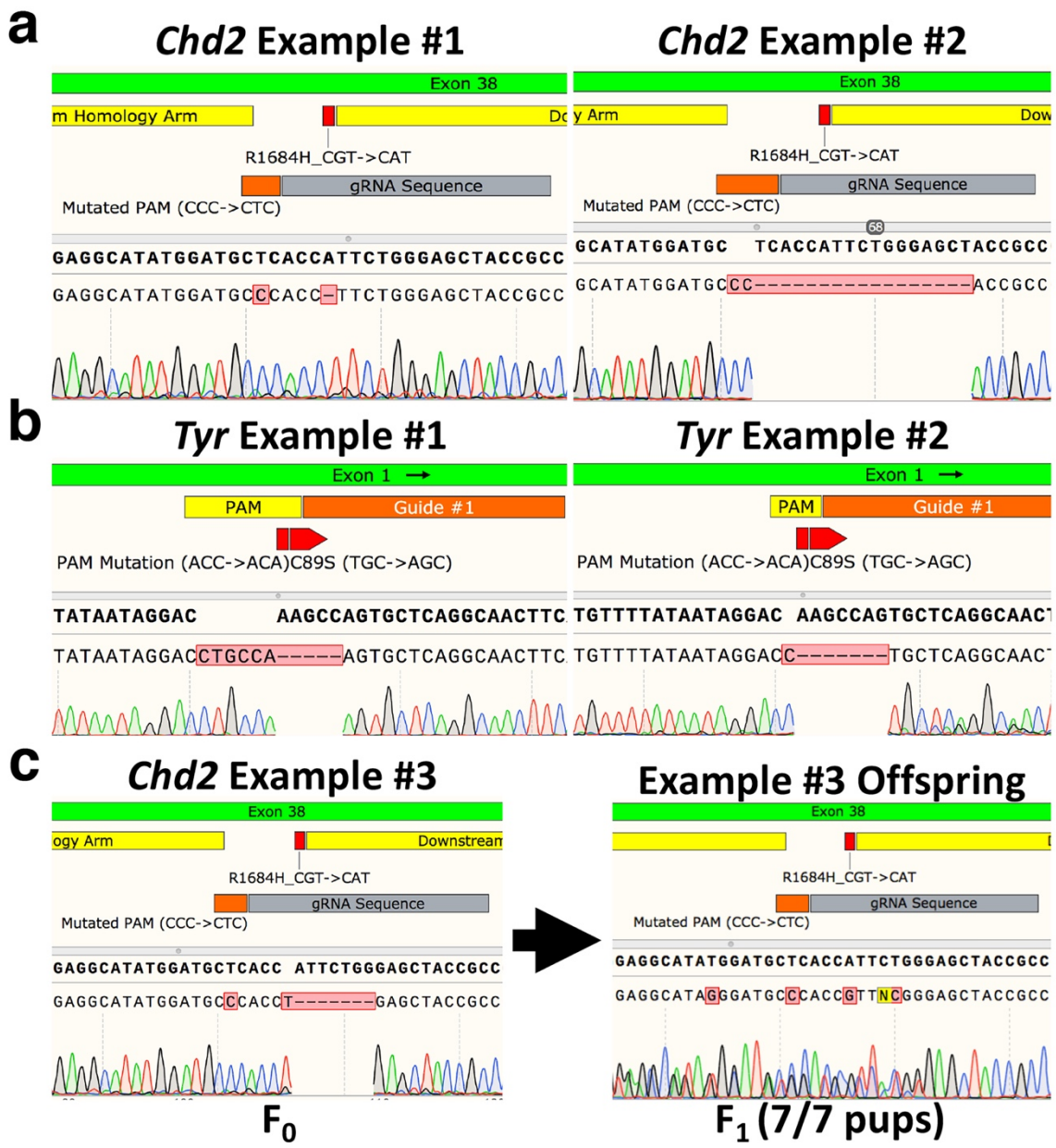

Extended Data Figure 3: RAD51 stimulates the generation of homozygous indels. a, Representative Sanger sequencing traces of putative homozygous indels observed in F_0 animals obtained from *Chd2*^{R1684H} knock-in experiments. **b,** Representative Sanger sequencing traces of putative homozygous indels observed in F_0 animals obtained from *Tyr*^{C89S} knock-in experiments. **c,** Genotyping traces for a putative homozygous *Chd2* indel and an F_1 offspring from a cross between the founder and a wildtype C57BL/6N mate. The F_1 genotyping, which was consistent for all 7 pups in the litter, indicates heterozygous presence of the indel observed in the founder.

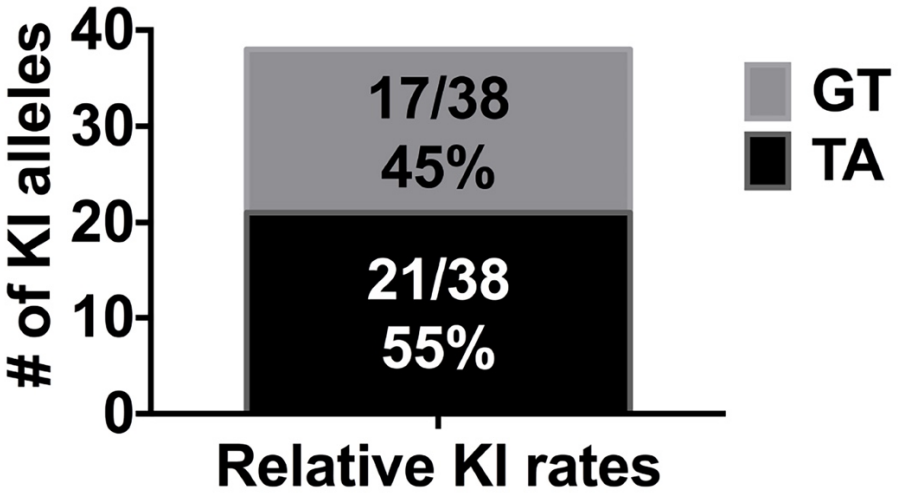

Extended Data Figure 4: TA (*Chd2*^{R1684H}) and GT donors show unbiased knock-in efficiencies. Quantification of KI rates observed for the TA (standard *Chd2*^{R1684H} donor) and GT donors used in Figure 2d shows no significant difference (two-tailed chi-square test).

Component	Sequence
tracrRNA	AAACAGCAUAGCAAGUUAAAAUAAGGCUAGUCCGU UAUCAACUUGAAAAAGUGGCACCGAGUCGGUGCU
Chd2^{R1684H} crRNA	GCGGUAGCUCCCAGAACGGUGUUUUAGAGCUAUGC UGUUUUG
Chd2^{R1684H} ssODN	TCAGTATGAGCAGCATTGGTATAAGGACCACCACTA TGGTGACCGGAGGCATATGGATGCTCACCATTCTGG GAGCTACCGCCCTAACAACATGTCCAGAAAGAGGCC GTATGAGCAGTACAACAG
Chd2^{GT} Variant Donor	TCAGTATGAGCAGCATTGGTATAAGGACCACCACTA TGGTGACCGGAGGCATATGGATGC CACCTTTCTGG GAGCTACCGCCCTAACAACATGTCCAGAAAGAGGCC GTATGAGCAGTACAACAG
Tyr^{C89S} crRNA	GAAGUUGCCUGAGCACUGGCGUUUUAGAGCUAUGC UGUUUUG
Tyr^{C89S} ssODN	GTTCCCCTTCAAAGGGGTGGATGACCGTGAGTCCTGG CCCTCTGTGTTTTATAATAGGACAAGCCAGTGCTCAG GCAACTTCATGGGTTTCAACTGCGGAAACTGTAAGTT TGGATTTGGGG

Supplementary Table 1: Sequences of Injection Components. Guide sequences are highlighted in red.

505

Forward Primer	Sequence	Reverse Primer	Sequence	Product Size (bp)
Chd2-RH_Long_F	ACTGACACATGGGAGAAGCC	Chd2-RH_Long_R	TCTCCTTATAACAGGCCAACC	429
Chd2-RH_F	AGTGCCTCACCTCTCACACC	Chd2-RH_R	ACTGGCAGAGGGAAAGAAAG	266
Tyr_Long_F	TCAATTTAGTTACCTCACTATGGGC	Tyr_Long_R	CAAGTACTCATCTGTGCAAATGTC	992
Tyr_F	TTTGGCCATAGGTGCCTG	Tyr _R	GAGCCTGTGCCTCCTCTAAG	411
Shank3_Long_F	AGGAAAGCAAGGTTGAGCTG	Shank3_Long_R	CTCTGAGGCTTGCAGACGG	584
Shank3_F	GAGCTCTACTCCCTTAGGACTT	Shank3_R	TCCCCCTTTCACTGGACACCC	316
Gapdh_Long_F	TACGGGTGCACGTAGCTCAG	Gapdh_Long_R	CGAAGGACACCAGGCAGTC	396
Gapdh_F	TCCCTAGACCCGTACAGTGC	Gapdh _R	CTCTGCTCCTCCCTGTTCC	133

506
507 **Supplementary Table 2: Sequences of PCR primers and expected product sizes.**
508
509
510
511
512
513
514
515
516
517
518
519
520
521
522
523
524
525
526
527
528
529
530